THE JOURNAL OF PHYSICAL CHEMISTRY C

Article

pubs.acs.org/JPCC

Sulfate Adsorption at the Buried Fluorite–Solution Interface Revealed by Vibrational Sum Frequency Generation Spectroscopy

Aaron M. Jubb and Heather C. Allen*

Department of Chemistry and Biochemistry, The Ohio State University, Columbus, Ohio 43210, United States

Supporting Information

ABSTRACT: Understanding the structure and energetics of adsorbed ions at buried mineral/solution interfaces has great importance to the geochemical and atmospheric chemistry communities. Vibrational spectroscopy is a powerful tool for the study of mineral/solution interfaces as these techniques can be applied in situ, are sensitive to surface structures, and are generally nondestructive. The use of vibrational sum frequency generation spectroscopy (VSFG), which is inherently interface-specific, is applied here to study the adsorption of sulfate at the buried fluorite (CaF_2)/Na_2SO_4 solution surface at pH 7 and 298 K in the presence of an aqueous background electrolyte, NaCl. The use of VSFG allowed for the resolution of adsorbed sulfate complexes from sulfate molecules which reside in the interfacial electric double layer yet remain fully solvated. The sulfate anion is found to adsorb with a bidentate inner-sphere structure at the fluorite surface with an average surface free energy of adsorption of -31 ± 3 kJ/mol for pH 7 solutions at 298 K.

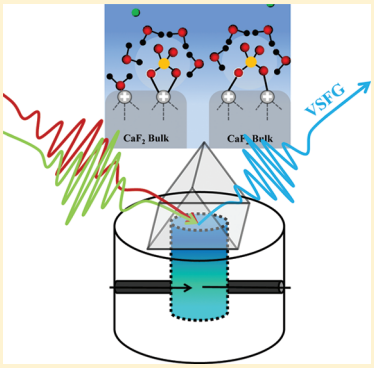

INTRODUCTION

Interactions that occur between charged mineral surfaces and aqueous ions play a large role in geochemical and atmospheric phenomena such as the uptake and retention of environmental contaminants by soils[1] as well as the reaction and growth of mineral dust aerosols.[2−4] These interactions also have industrial implications for processes such as mineral ore flotation.[5,6] Despite the importance of surface interactions occurring at or near mineral/solution interfaces, characterization of the interfacial chemistry for such systems remains difficult. Analytical methods used to study mineral−ion interactions at buried mineral/solution interfaces typically involve batch and column experiments,[7,8] vibrational spectroscopic techniques such as infrared and Raman spectroscopies,[9−16] ultrahigh vacuum techniques,[17,18] and X-ray absorption spectroscopies.[19−21] These experimental studies have been complemented by theoretical work which has helped elucidate many long-standing questions with regard to adsorption structure and thermodynamics.[22−25]

Sulfate adsorption onto mineral surfaces, predominantly oxide minerals, from aqueous solution has been reported widely within the literature utilizing a variety of analytical methods.[11,12,14,15,23,26−28] Much of this work has focused on applying infrared and Raman spectroscopies to distinguish sulfate adsorption structure. Vibrational spectroscopic techniques are appealing as these methods can be carried out at standard temperatures and pressures, are capable of in situ measurements during flow or exposure experiments, and are generally nondestructive of the sample.[9−14,16] Sulfate (SO_4^{2-}) is a simple, inorganic anion whose behavior is important to understand as it is ubiquitous in the environment being the third most prevalent ionic chemical species in seawater by weight.[29] It is also the end oxidation product of sulfur containing chemical species and has been linked to the growth of tropospheric aqueous aerosols.[2,30] From a geochemical perspective, sulfate adsorption to mineral surfaces is important as it can compete with less environmentally benign aqueous anions such as selenate (SeO_4^{2-}), selenite (SeO_3^{2-}), chromate (CrO_4^{2-}), etc. for adsorption sites within contaminated soils increasing the mobility of these toxic compounds.[1]

Here we report for the first time, using vibrational sum frequency generation (VSFG) spectroscopy, the direct observation of sulfate adsorption at the buried mineral/solution interface as revealed by the adsorbed anion's vibrational stretching modes. Previous to this, Morita and co-workers have demonstrated the power of VSFG to directly interrogate bisulfate ion vibrational modes at vapor/solution interfaces.[31,32] We have investigated the interaction and subsequent adsorption of the sulfate anion at the charged fluorite (CaF_2)/Na_2SO_4 solution interface at pH 7 and 298 K in the presence of a 1 molal NaCl background electrolyte for a range of Na_2SO_4 solution concentrations. We compare our VSFG results to conventional infrared and Raman spectroscopic results for bulk aqueous Na_2SO_4 solution and solid Na_2SO_4. A discussion of the sulfate adsorption structure and surface free energy of adsorption at the fluorite surface determined from the VSFG results follows. These findings may help provide physical insight into various geochemical and atmospheric phenomena such as the comparatively large disordering effect that aqueous sulfate has on water's hydrogen bond network near charged

Received: February 6, 2012
Revised: March 28, 2012
Published: April 3, 2012

mineral surfaces[33] as well as the retardation of mineral dust aerosol ice nucleation by sulfate coatings.[3,4,34,35]

Fluorite was chosen as the mineral substrate due to its importance as an industrial mineral being the main source for production of hydrofluoric acid by reaction with sulfuric acid.[36] Fluorite also has many experimentally necessary qualities for VSFG studies of ion interactions at mineral/solution interfaces. These qualities include a large transmission range in the visible and infrared frequency ranges as well as a small aqueous solubility (1.6×10^{-3} g/100 g H_2O at 25 °C).[37] The ideal surface terminations of fluorite in contact with water were determined by Wu et al.[5] via a thermodynamic equilibrium model and have been summarized in a later publication by Schrödle et al. for a range of pH values.[38] At a pH value of 7 the ideal fluorite surface terminations should be two calcium centers coordinated to either water or fluoride. While the reported isoelectric point of fluorite has a broad range, an approximate working value of 8 is assumed here following the findings of Wu et al. and Schrödle et al.[5,38] Hence it can be surmised that for pH values less than 8 the fluorite surface should feature a net positive charge. These qualities make fluorite an ideal model to study the adsorption behavior of sulfate from aqueous solution onto charged mineral surfaces.

The strength of vibrational spectroscopic techniques to study ion behavior at mineral/solution interfaces in situ was first demonstrated in 1997 by Hug[12] who utilized an attenuated total reflection (ATR) element coated with colloidal hematite particles to study sulfate adsorption on the hematite particle surface via infrared spectroscopy. While Hug's insights into using an ATR-infrared approach to study mineral−ion systems have been widely adopted,[9,11,14,15,26,28] an inherent weakness of linear spectroscopic techniques is their lack of interfacial specificity. This may result in the collected spectra containing information from bulk solvated ions as well as the adsorbed chemical species of interest.

More recently, nonlinear spectroscopic techniques such as VSFG have been applied to study buried mineral/solution interfaces, predominantly with perspective toward elucidating interfacial water structure near charged mineral surfaces.[33,35,39−47] Taking advantage of third-order susceptibility ($\chi^{(3)}$) effects from water near charged mineral interfaces, several research groups have also indirectly probed aqueous ion behavior at buried mineral/solution interfaces via VSFG and second harmonic generation (SHG) spectroscopies.[42,43,48,49] However, the application of nonlinear spectroscopic techniques to directly study adsorption at charged mineral/solution interfaces has seen limited adoption.[30,38,48,50−54] VSFG reports of this nature are generally lacking due to increased experimental difficulties associated with accessing buried interfaces and producing input infrared frequencies at the low frequencies required to directly probe the ion vibrational modes of interest. While the increased experimental difficulties of the VSFG technique put it at a disadvantage for studying buried interfaces when compared to the relatively more straightforward ATR-infrared and Raman techniques, it has a large advantage in that it is inherently interface-specific.[55] This specificity makes it possible to resolve spectral features associated with the adsorbed species of interest from nonadsorbed interfacial chemical species residing within the electric double layer near the mineral surface.

EXPERIMENTAL METHODS

VSFG Theory. VSFG spectroscopy is an even-order nonlinear vibrational technique that can provide molecular level information of interfaces. It relies on the nonlinear response induced by the spatial and temporal overlap of two input beams (typically at visible and infrared frequencies) at an interface. The frequency of the generated nonlinear beam occurs at the sum of the two input beam frequencies. The intensity of the VSFG response is proportional to the effective second-order nonlinear susceptibility ($\chi^{(2)}_{\mathrm{eff}}$) of VSFG active oscillators in resonance with an input beam frequency, generally the infrared beam, and to the intensities of the two input beams[55,56]

$$I_{\mathrm{VSFG}} \propto |\chi^{(2)}_{\mathrm{eff}}|^2 I_{\mathrm{Vis}} I_{\mathrm{IR}} \propto |\chi^{(2)}_{\mathrm{eff,NR}} + \sum_{\nu} \chi^{(2)}_{\mathrm{eff},\nu}|^2 I_{\mathrm{Vis}} I_{\mathrm{IR}} \quad (1)$$

where $\chi^{(2)}_{\mathrm{eff,NR}}$ and $\chi^{(2)}_{\mathrm{eff},\nu}$ are the nonresonant and resonant contributions of $\chi^{(2)}_{\mathrm{eff}}$, respectively. The resonant contribution $\chi^{(2)}_{\mathrm{eff},\nu}$ is given by

$$\chi^{(2)}_{\mathrm{eff},\nu} = N_s \sum_{lmn} \langle \mu_{IJK:lmn} \rangle \beta_{lmn,\nu} \quad (2)$$

where N_S is the surface number density of VSFG active oscillators; $\beta_{lmn,\nu}$ is the molecular hyperpolarizability; and $\langle \mu_{IJK:lmn} \rangle$ is the orientationally averaged Euler angle transformation between laboratory (IJK) and molecular (lmn) coordinates. The molecular hyperpolarizability, $\beta_{lmn,\nu}$, is proportional to the Raman polarizability tensor for the transition moment $\langle g|\alpha_{lm}|\nu\rangle$ and the infrared transition moment $\langle \nu|\mu_n|g\rangle$, eq 3, which results in the selection rule for VSFG activity that a vibration must be both Raman and infrared active.

$$\beta_{lmn,\nu} = \frac{\langle g|\alpha_{lm}|\nu\rangle\langle \nu|\mu_n|g\rangle}{\omega_{\mathrm{IR}} - \omega_\nu + i\Gamma_\nu} \quad (3)$$

VSFG Instrumentation. The VSFG spectra were acquired using a 20 Hz scanning VSFG system (EKSPLA). The VSFG experiments were carried out using a fixed frequency visible beam at 532 nm and a tunable frequency infrared beam scanned from 950 to 1250 cm^{-1} during the course of a spectral acquisition. The 532 nm beam is generated by doubling the frequency (second harmonic) of the 1064 nm fundamental output from an Nd:YAG laser (25 ps pulse duration and 20 Hz repetition rate) (EKSPLA, PL2143A/20/SS). The tunable infrared beam is produced from an optical parametric generator (OPG) (EKSPLA, PG401/DFG2-16P) using a GaSe crystal to generate the infrared beam via the difference frequency mixing of the 1064 nm fundamental from the Nd:YAG with a tunable idler beam produced in the first stage of the OPG. The 532 nm light is focused 40 mm after the sample stage by using a plano-convex lens (700 mm focal length). The infrared beam is focused at the sample stage using a ZnSe lens (50 mm focal length).

All VSFG spectra shown were collected using an experimental geometry, Figure 1, where both the visible and infrared input beams are transmitted to the fluorite/solution interface through an equilateral fluorite prism mounted on a custom-made Teflon flow cell (complete flow cell details in Supporting Information). The 532 nm and infrared beams are overlapped at the fluorite/Na_2SO_4 solution interface both spatially and temporally. The incident angles for the visible and infrared input beams are 70° and 65°, respectively, relative to

dx.doi.org/10.1021/jp301186w | J. Phys. Chem. C 2012, 116, 9085−9091

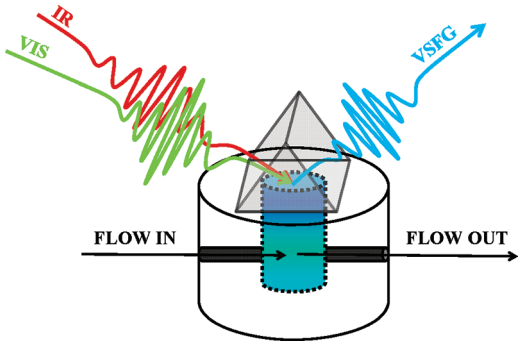

Figure 1. Experimental flow cell showing the fluorite prism in contact with the sample solution with input visible and infrared beam and generated VSFG beam geometries noted.

the normal of the fluorite/Na_2SO_4 interface. For the visible beam, the chosen angle is large enough to achieve the total internal reflection condition which has been shown to yield drastically higher S/N ratios.[57] The input energies of the visible and infrared beams during a typical VSFG spectral acquisition are generally ~300 and ~100 μJ/pulse, respectively. All VSFG spectra shown were collected with 5 s of acquisition at each data point with an electron multiplying gain of 100 applied to the CCD. The generated sum frequency light is collected using a cooled electron multiplying charge coupled device (EMCCD) camera (Andor Technology, Newton, DU97ON-BV). The polarization combinations used in this study were SSP and PPP where the first letter is the sum frequency; the second is the visible; and the last letter represents the infrared beam, respectively. Here S polarized light signifies that the electric field vector of the respective beam is perpendicular to the plane of incidence, while P polarized light has its electric field vector parallel to the plane of incidence.

For the VSFG experiments, the Na_2SO_4 solutions are purged with house $N_{2(g)}$ to remove dissolved $CO_{2(g)}$ until the pH of the solution is 7 before use. The Na_2SO_4 solutions are then pumped to the fluorite/Na_2SO_4 interface via a peristaltic pump (MasterFlex L/S, Cole-Parmer). The solutions were allowed to equilibrate with the fluorite surface for 10 m before the VSFG spectra were collected. The pH of each solution was checked (Ag/AgCl glass electrode, Accumet AB15, Fisher Scientific) before and after each VSFG spectrum was collected to ensure that the pH did not change during the course of the experiment. The pH meter was calibrated following the procedure of Wiesner et al. for high ionic strength solutions.[58] Between experimental runs, the flow cell was flushed with N_2-purged nanopure water (18.3 MΩ) until the adsorbed sulfate signal was no longer detectable to ensure the reversibility of the adsorption process.

The collected VSFG spectra were normalized to the input 532 nm and infrared beam intensities, simultaneously detected with the VSFG spectra, and then normalized against the transmission curve for fluorite. The presented VSFG spectra are the average of 3−4 spectra. All VSFG spectra have been calibrated against the VSFG spectrum of the SO_3 symmetric stretching peak at 1070 cm^{-1} of a sodium dodecyl sulfate (SDS) monolayer on neat water collected at the beginning and end of each day experiments were run.[59]

Raman and Infrared Instrumentation. The Raman experiments were carried out using a 532.1 nm continuous-wave diode-pumped Nd:YVO_4 laser (Millennium II, Spectra-Physics) with a parallel (P) input beam polarization and a power of 100 mW. All experiments were carried out with 30 s acquisition time with the collected Raman signal sent to a monochromator (SpectraPro 500i, Princeton Instruments) equipped with a 1200 groove/mm grating and detected on a liquid N_2-cooled deep-depletion CCD (1340/400-EB, Roper Scientific). The infrared spectra were collected utilizing a home-built ATR apparatus using a ZnSe element to achieve total internal reflection of the infrared beam. This apparatus was mounted in a conventional benchtop FTIR instrument (Spectrum 100, Perkin-Elmer). The infrared spectra shown are the average of 400 scans normalized against a background spectrum of neat water (Figure 2a) or of the bare ZnSe element (Figure 2b).

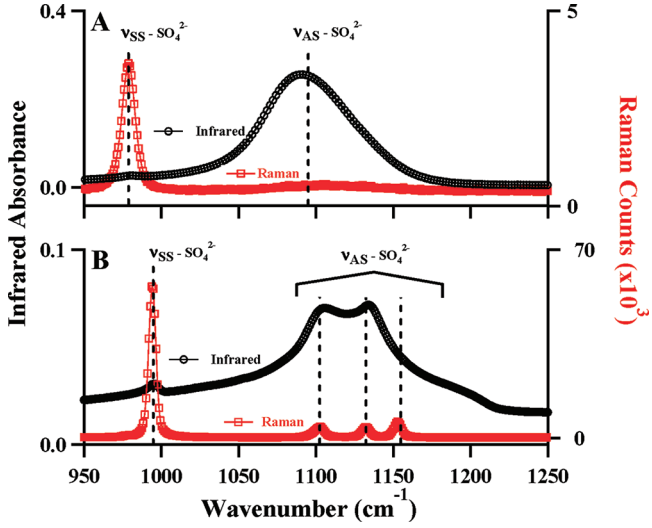

Figure 2. Normalized infrared and Raman spectra from (A) 1 m Na_2SO_4 solutions at pH 7 and 298 K and (B) solid, anhydrous Na_2SO_4 at 298 K. Spectral assignments are indicated above the respective peaks. Vertical dashed lines indicate respective peak centers.

Chemicals. Molality (m), which is defined here as moles of solute per kilogram of water, is used as the concentration unit for the Na_2SO_4 solutions prepared. Solutions of Na_2SO_4 of various molality were prepared by mixing solid Na_2SO_4 (99+% pure, Acros Organics, crystalline, anhydrous), annealed at 600 °C for 4 h to remove organic impurities, and nanopure water (18.3 MΩ, NanoPure, Barnstead/Thermolyne) to the desired concentration with an appropriate amount of solid NaCl (≥99.5% pure, Sigma-Aldrich), also annealed at 600 °C for 4 h, to bring the background electrolyte concentration to approximately 1 m NaCl. The equilateral fluorite prism (25 × 25 × 25 mm, flatness ±10 min, 40/20 surface finish) was purchased from ISP Optics Inc. and was cleaned by sonication in dry methanol (reagent grade, Sigma-Aldrich) followed by copious rinsing with nanopure water before use. The SDS solution used for calibration of the VSFG spectra was prepared from solid SDS powder (99+% pure, ACS reagent grade, Sigma-Aldrich) and nanopure water.

RESULTS AND DISCUSSION

The infrared and Raman spectra of a 1 m Na_2SO_4 solution in the S−O stretching region from 950 to 1250 cm^{-1} are shown in Figure 2a. Both spectra exhibit the expected sulfate vibrational mode peaks with the Raman spectrum featuring a strong peak at 980 cm^{-1} corresponding to the symmetric stretch (ν_{SS}-

dx.doi.org/10.1021/jp301186w | J. Phys. Chem. C 2012, 116, 9085−9091

SO_4^{2-}) of solvated sulfate and a weak, broad feature centered at ~1100 cm^{-1} assigned to the triply degenerate asymmetric stretching (ν_{AS}-SO_4^{2-}) modes of sulfate.[12,60,61] The infrared spectrum in Figure 2a exhibits a very strong peak centered at 1090 cm^{-1}, assigned to the degenerate ν_{AS}-SO_4^{2-} modes of solvated sulfate, consistent with literature.[12] From the spectra shown in Figure 2a little to no VSFG activity is predicted for the fully solvated or "free" sulfate vibrational modes as neither ν_{SS}-SO_4^{2-} nor ν_{AS}-$SO_4^{2-}$is strongly Raman and infrared active, indicating weak hyperpolarizabilities for these vibrational modes (eq 3) when sulfate possesses T_d symmetry.[55] However, upon inner-sphere adsorption, it is expected that the sulfate anion symmetry will lower from T_d resulting in both ν_{SS}-SO_4^{2-} and ν_{AS}-SO_4^{2-} becoming Raman and infrared active and as such VSFG active as well.[12]

This symmetry lowering is the basis for the determination of sulfate adsorption structure at mineral surfaces via ATR-FTIR.[9,11,12,14,26] For T_d symmetry the triple degeneracy of ν_{AS}-SO_4^{2-} results in one broad strong peak observed in the infrared spectrum (Figure 2a). Upon inner-sphere adsorption, the sulfate symmetry will lower to C_{3v} or C_{2v} resulting in two or three distinct frequencies observed for the ν_{AS}-SO_4^{2-} modes, respectively.[11,12] As shown in Figure 2b, three peaks are observed for the ν_{AS}-SO_4^{2-} modes in both the Raman and infrared spectra of solid Na_2SO_4, illustrating the symmetry lowering effects of coordination for the sulfate S−O stretching modes. Also apparent is the blue shift of the ν_{SS}-SO_4^{2-} mode from 980 to 993 cm^{-1}, along with ν_{SS}-SO_4^{2-} becoming infrared active consistent with a C_{2v} or lower symmetry for the sulfate anion. From Figure 2b, it may be surmised that upon inner-sphere adsorption to the fluorite surface the sulfate anion's stretching vibrations should become VSFG active as adsorption will lower the sulfate anion symmetry such that ν_{SS}-SO_4^{2-} and ν_{AS}-SO_4^{2-} will become Raman and infrared active. Upon the basis of the number and frequency of these modes, the adsorption structure for sulfate at the fluorite surface can then be inferred.

Shown in Figure 3 are the VSFG results for sulfate adsorption at the fluorite surface from Na_2SO_4 solutions ranging in concentration from 0.1 mm to 100 mm in the presence of a 1 m NaCl background electrolyte at pH 7 and 298 K. The background electrolyte is necessary to ensure that the total ionic strength of the solution does not change significantly with an increase in Na_2SO_4 concentration as this will affect the effective charge of the fluorite surface.[62] Two separate polarization combinations (SSP and PPP) were used to probe sulfate adsorption at the fluorite surface (Figure 3a, b). The markers in Figure 3 correspond to the data, while the solid lines represent the best fits to the data (see Supporting Information for fitting details).

In Figure 3a and 3b, sulfate adsorption becomes discernible for the lowest concentration solution tested, 0.1 mm, with two weak peaks centered at ~1115 and ~1160 cm^{-1} for the SSP spectrum and ~1095 and ~1145 cm^{-1} for the PPP spectrum appearing. These peaks correspond to the two strongest ν_{AS}-SO_4^{2-} modes of the bound sulfate anion. The ν_{SS}-SO_4^{2-} peak is most likely not resolvable for the 0.1 mm Na_2SO_4 solutions due to a combination of low sulfate concentration and the lower infrared transmission of fluorite at 1000 cm^{-1} compared to 1150 cm^{-1}. As Na_2SO_4 concentration increases above 0.1 mm, the VSFG response dramatically increases until four peaks are observed in both the SSP and PPP VSFG spectra. The mode centered at 990 cm^{-1} in both Figure 3a and 3b is assigned to

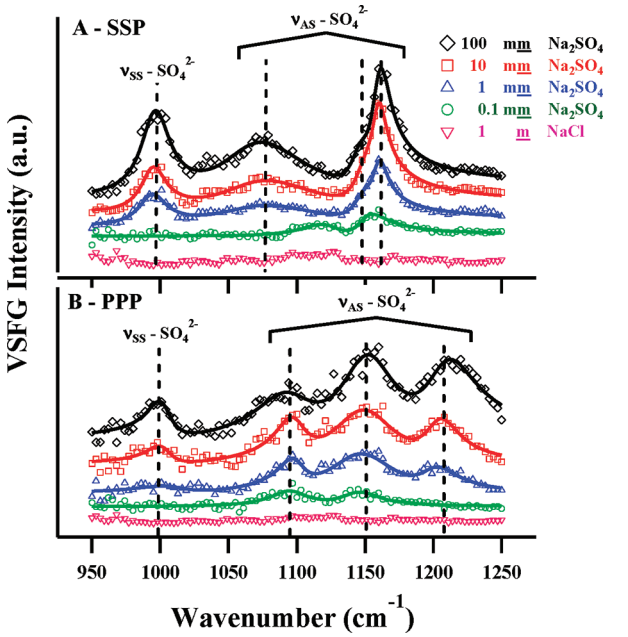

Figure 3. Normalized VSFG spectra (A - SSP and B - PPP) of the CaF_2/Na_2SO_4 solution interface for a range of Na_2SO_4 concentrations in 1 m NaCl background electrolyte at pH 7 and 298 K. Spectral assignments are indicated above the peaks. The markers are data, and solid lines are best fits to the data. Spectra offset for clarity. Vertical dashed lines indicate respective peak centers.

the ν_{SS}-SO_4^{2-} mode of adsorbed sulfate surface complexes. The three higher-frequency modes present in Figure 3 are assigned to the nondegenerate ν_{AS}-SO_4^{2-} modes of sulfate surface structures.[12]

Figure 4 gives a schematic of five possible ideal surface structures that sulfate could adopt at the fluorite surface ranging from a nonbonding interaction to bidentate surface complexes where two of the sulfate anion's oxygens bond directly with a positive calcium center surface site. The symmetry of each representative sulfate surface structure is indicated below the scheme shown in Figure 4, and the net effect on the sulfate anion charge is noted. For schemes I and II, corresponding to the noninteractive fully solvated sulfate anion and an outer-sphere hydrogen-bound sulfate anion, respectively, no VSFG activity is expected as in these environments the sulfate anion will retain T_d symmetry. In scheme III, representing monodentate inner-sphere sulfate adsorption, the sulfate anion possesses C_{3v} symmetry which will incompletely lift the degeneracy of the ν_{AS}-SO_4^{2-} modes, resulting in two distinct frequencies for these vibrations. Hence for sulfate surface complexes possessing C_{3v} symmetry, three total VSFG peaks would be expected, two ν_{AS}-SO_4^{2-} peaks and the ν_{SS}-SO_4^{2-} peak. The final two schemes, IV and V, represent monatomic and bridging bidentate inner-sphere sulfate structures, respectively. For both of these structures, the sulfate anion symmetry will lower to C_{2v}, which completely breaks the ν_{AS}-SO_4^{2-} degeneracy, resulting in three distinct stretching frequencies. Thus, for bidentate inner-sphere sulfate coordination at the fluorite surface, four total VSFG peaks are expected.

As discussed above, four peaks are observed for both SSP and PPP polarization combinations for the three most concentrated Na_2SO_4 solutions (Figure 3a, b) indicating net C_{2v} symmetry for the adsorbed sulfate structures. While the SSP spectra are best fit with four peaks for all but the weakest Na_2SO_4

dx.doi.org/10.1021/jp301186w | J. Phys. Chem. C 2012, 116, 9085−9091

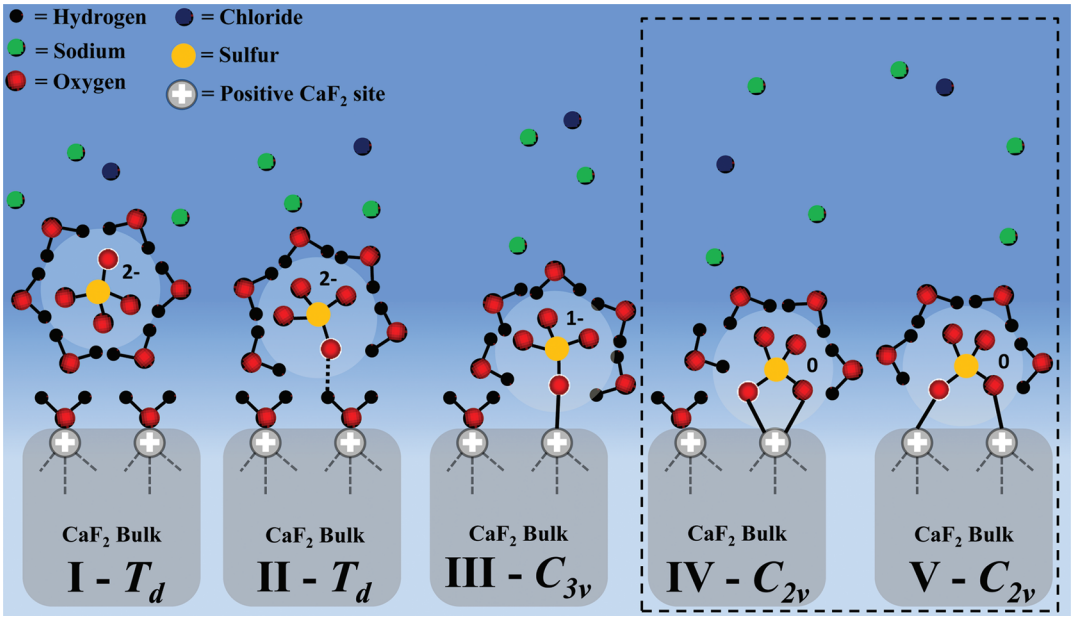

Figure 4. Cartoon representation of possible interaction schemes for SO_4^{2-} at the CaF_2/Na_2SO_4 solution interface with symmetry of the sulfate anion for each scheme indicated next to the Roman numeral. Note that the blue background represents bulk aqueous solution. Scheme I: noninteracting. Scheme II: outer-sphere coordination. Scheme III: monodentate inner-sphere coordination. Scheme IV: monatomic bidentate inner-sphere coordination. Scheme V: bridging bidentate inner-sphere coordination. Schemes IV and V are boxed to indicate preferred sulfate adsorption structure at the fluorite surface. The effective charge of the SO_4^{2-} anion is noted for each possible surface structure beside the sulfur atom of SO_4^{2-}. Dashed line in Scheme II represents a hydrogen bond. Solid lines in Schemes III, IV, and V represent a direct bond with the fluorite surface site.

concentration solution tested, the peak frequencies are not as distinct as those observed in the PPP spectra (Figure 3b). By utilizing different VSFG polarization schemes, it is possible to probe different sulfate adsorption structures which may feature varying distributions at the fluorite surface. These subdistributions of sulfate adsorption structures will preferentially interact with a specific input beam polarization combination due to geometric alignment with the electric-field vectors of the input beams. This alignment will result in the detected sum frequency response for different polarization combinations having greater signal contribution from the preferred subdistribution of adsorption structures. The presence of varying sulfate adsorption structures is apparent when comparing the ν_{AS}-SO_4^{2-} mode frequencies between the SSP and PPP spectra shown in Figure 3, which clearly vary, even though both spectra sets indicate C_{2v} symmetry for the adsorbed sulfate. Sulfate's ν_{AS}-SO_4^{2-} vibrational frequencies are known to vary significantly with molecular environment, even for sulfate anions possessing the same symmetry group, and as such the VSFG spectra in Figure 3 reflect the differing distributions of sulfate adsorption structures at the fluorite/solution interface.[63] These distributions, which manifest as frequency differences for the ν_{AS}-SO_4^{2-} modes, make a detailed analysis of the net sulfate adsorption structure orientation infeasible.

The clear presence of four peaks in the SSP and PPP spectra indicates that sulfate adsorbs to the fluorite surface predominantly in a bidentate inner-sphere manner consistent with schemes IV or V shown in Figure 4. While it is not possible from the VSFG data to distinguish between monatomic versus bridging bidentate coordination, the presence of four peaks clearly indicates that a bidentate adsorption structure is preferred by sulfate at the fluorite surface. In both the SSP and PPP spectra, sulfate adsorption is clearly present for the lowest Na_2SO_4 concentration tested (0.1 mm), indicating that the sulfate anion forms surface adsorption complexes with fluorite even from dilute solutions at 298 K and pH 7.

It is possible to calculate the net free energy of adsorption for the bidentate inner-sphere sulfate complexes by applying a simple Langmuir adsorption model to the SSP and PPP data.[48,50,62] An important consideration when applying this model to VSFG studies is that the detected VSFG intensity is proportional to the orientation of the adsorbed species as well as the surface number density (see eq 2). For the purposes of this analysis, it is reasonable to assume that the net orientation of the sulfate bidentate inner-sphere complexes remains constant as the concentration of Na_2SO_4 increases. Figure 5 shows the Langmuir adsorption isotherms generated by plotting the square-root of the detected VSFG intensities for the ν_{SS}-SO_4^{2-} peak and the strongest ν_{AS}-SO_4^{2-} peak for both the SSP and PPP data sets versus Na_2SO_4 solution concentration. Table 1 details the results of the Langmuir adsorption analysis, with an average $\Delta G^\circ_{ads} = -33 \pm 2$ kJ/mol (rounded to the nearest whole number) determined when fitting all four Na_2SO_4 concentrations and $\Delta G^\circ_{ads} = -29 \pm 2$ kJ/mol when fitting just the three most concentrated Na_2SO_4 solutions (see Supporting Information for details). The Langmuir analysis was carried out for just the three most concentrated Na_2SO_4 solutions for comparison purposes as the 0.1 mm solution VSFG peak intensities have the highest uncertainty due to the weakness of the VSFG response for this Na_2SO_4 concentration.

While the limited number of Na_2SO_4 concentrations tested and the assumption of constant orientation for the adsorbed surface structures make the application of a Langmuir adsorption analysis here somewhat physically questionable, the agreement between the calculated adsorption free energies between the SSP and PPP data when both four and three Na_2SO_4 concentrations were fit (Table 1) indicates that a Langmuir analysis is not completely unreasonable. Thus, an

dx.doi.org/10.1021/jp301186w | J. Phys. Chem. C 2012, 116, 9085−9091

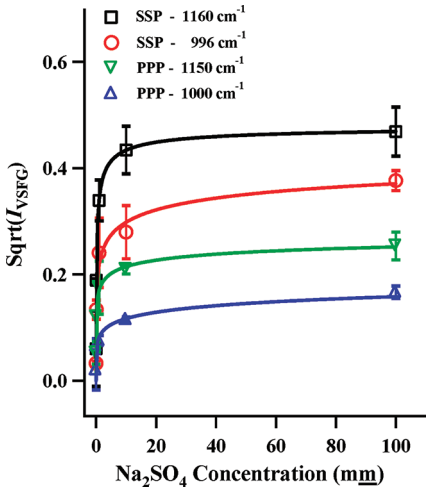

Figure 5. Langmuir adsorption isotherms generated by plotting the square-root of the VSFG peak intensity versus Na_2SO_4 solution concentration. Peaks chosen correspond to the 996 and 1160 cm^{-1} peaks for the SSP data and 1000 and 1150 cm^{-1} peaks for PPP data. Markers are data; error bars are plus/minus one standard deviation; and solid lines are fits using the Langmuir equation.

average value of −31 ± 3 kJ/mol is proposed as a first-approximation for the ΔG°_{ads} for sulfate at the fluorite surface. It is also worth noting that an average value for $\Delta G^\circ_{ads} = -31 \pm 3$ kJ/mol, which is approximately as strong as several hydrogen bonds, is quite reasonable considering the reversibility of sulfate adsorption at the fluorite surface and is in good agreement with literature values for reversible simple inorganic ion adsorption at charged mineral surfaces.[48−50]

These findings help explain recent work on resolving water structure near the charged fluorite surface for a variety of simple inorganic salt solutions, including Na_2SO_4, carried out by Hopkins et al.[33] In this study, the presence of Na_2SO_4 was observed to retard the ordering effects of the charged fluorite surface on interfacial water to a greater degree than was observed for other inorganic salts (NaCl, NaBr, and NaF) tested, beyond what would be predicted by Gouy−Chapman theory.[33,62] The VSFG results presented here, indicating that sulfate predominantly forms bidentate inner-sphere adsorption complexes with the fluorite surface, provides insight into the underlying physical forces behind the water disordering effects observed at the fluorite/sulfate solution interface by Hopkins et al. In forming bidentate inner-sphere adsorption complexes at the fluorite surface, sulfate not only replaces adsorbed water at the fluorite surface but also effectively removes the net charge of the positive fluorite surface terminations. This reduces the local electric field responsible for water ordering near a charged mineral surface to a greater degree than what could be expected for nonbinding ions near the mineral surface. This is a plausible explanation for the observed reduction of interfacial water ordering at the fluorite/solution interface by aqueous sulfate beyond what would be predicted by Gouy−Chapman theory.[33,62]

CONCLUSIONS

The direct observation of sulfate adsorption to a charged mineral, fluorite (CaF_2), surface at the buried mineral/solution interface is reported for the first time using VSFG spectroscopy. The use of VSFG to study adsorption phenomena at buried interfaces has the advantage over conventional vibrational spectroscopic techniques in that it is inherently interface-specific, allowing for the resolution of adsorbed sulfate surface structures from nonbound fully solvated sulfate near the interface. Sulfate is found to predominantly adsorb in a bidentate inner-sphere manner with an average net surface free energy of adsorption for these complexes calculated to be $\Delta G^\circ_{ads} = -31 \pm 3$ kJ/mol using a Langmuir adsorption analysis. These findings have significance toward geochemical and atmospheric phenomena such as competition between sulfate and other aqueous anions for mineral adsorption sites as well as the water uptake and reaction of sulfate-coated mineral dust aerosols.[1,3] The application of the VSFG method toward the study of sulfate adsorption onto other environmentally relevant minerals at the buried mineral/solution interface is the subject of ongoing work.

ASSOCIATED CONTENT

Supporting Information

Includes the complete diagram of the VSFG experimental flow cell, the VSFG fitting parameters and results, and complete details of the Langmuir adsorption analysis. This material is available free of charge via the Internet at http://pubs.acs.org.

AUTHOR INFORMATION

Corresponding Author

*E-mail: allen@chemistry.ohio-state.edu.

Notes

The authors declare no competing financial interest.

ACKNOWLEDGMENTS

We acknowledge the DOE-BES Geochemistry (Grant No. DE-FG02-04ER15495) for funding this work. Dr. Ralf Posner is also acknowledged for his help with the VSFG experiments.

Table 1. Langmuir Adsorption Analysis Results

		with four concentrations fit		with three concentrations fit	
peak frequency (cm^{-1})	polarization	$d(1/\theta)/d(1/[SO_4^{2-}])^a$	ΔG°_{ads} (kJ/mol)^b	$d(1/\theta)/d(1/[SO_4^{2-}])^a$	ΔG°_{ads} (kJ/mol)^b
996	SSP	$(1.2 \pm 0.2) \times 10^{-4}$	−32.3 ± 0.4	$(3.3 \pm 2.1) \times 10^{-4}$	−29.8 ± 1.9
1160	SSP	$(1.3 \pm 0.1) \times 10^{-4}$	−32.1 ± 0.3	$(3.4 \pm 0.4) \times 10^{-4}$	−29.7 ± 0.3
1000	PPP	$(7.8 \pm 4.5) \times 10^{-5}$	−33.4 ± 1.6	$(7.3 \pm 2.2) \times 10^{-4}$	−27.9 ± 0.5
1150	PPP	$(7.8 \pm 1.8) \times 10^{-5}$	−33.4 ± 0.6	$(3.1 \pm 1.3) \times 10^{-4}$	−30.0 ± 1.1

[a]Slope of line-of-best fit for one over relative surface coverage (θ) vs one over Na_2SO_4 solution concentration from Figure S3 using four or three Na_2SO_4 concentrations (see Supporting Information for details), plus/minus one standard deviation. [b]Calculated surface free energy of adsorption using equation S2 (Supporting Information), plus/minus one standard deviation.

REFERENCES

(1) Langmuir, D. *Aqueous Environmental Geochemistry*, 1st ed.; Prentice Hall: Upper Saddle River, NJ, 1997.
(2) Finlayson-Pitts, B. J.; Pitts, J. N., Jr. *Chemistry of the Upper and Lower Atmosphere: Theory, Experiments, and Applications*, 1st ed.; Academic Press: San Diego, CA, 1999.
(3) Usher, C. R.; Michel, A. E.; Grassian, V. H. *Chem. Rev.* **2003**, *103*, 4883−4940.
(4) Cziczo, D. J.; Froyd, K. D.; Gallavardin, S. J.; Moehler, O.; Benz, S.; Saathoff, H.; Murphy, D. M. *Environ. Res. Lett.* **2009**, *4*, 044013.
(5) Wu, L.; Forsling, W. *J. Colloid Interface Sci.* **1995**, *174*, 178−184.
(6) *Flotation: A.M. Gaudin Memorial Vol.*; Fuerstenau, M. C., Ed.; American Institute of Mining, Metallugical, and Petroleum Engineers: New York, NY, 1976; Vol. *1*.
(7) Jia, Y.; Demopoulos, G. P. *Environ. Sci. Technol.* **2005**, *39*, 9523−9527.
(8) Hayes, K. F.; Papelis, C.; Leckie, J. O. *J. Colloid Interface Sci.* **1988**, *125*, 717−726.
(9) Yoon, T. H.; Johnson, S. B.; Musgrave, C. B.; Brown, G. E. *Geochim. Cosmochim. Acta* **2004**, *68*, 4505−4518.
(10) Uibel, R. H.; Harris, J. M. *Anal. Chem.* **2002**, *74*, 5112−5120.
(11) Lefèvre, G. *Adv. Colloid Interface Sci.* **2004**, *107*, 109−123.
(12) Hug, S. J. *J. Colloid Interface Sci.* **1997**, *188*, 415−422.
(13) Beattie, D. A.; Larsson, M. L.; Holmgren, A. R. *Vib. Spectrosc.* **2006**, *41*, 198−204.
(14) Eggleston, C. M.; Hug, S.; Stumm, W.; Sulzberger, B.; Dos Santos Afonso, M. *Geochim. Cosmochim. Acta* **1998**, *62*, 585−593.
(15) Wijnja, H.; Schulthess, C. P. *J. Colloid Interface Sci.* **2000**, *229*, 286−297.
(16) Tyrode, E.; Rutland, M. W.; Bain, C. D. *J. Am. Chem. Soc.* **2008**, *130*, 17434−17445.
(17) Brown, G. E.; Henrich, V. E.; Casey, W. H.; Clark, D. L.; Eggleston, C.; Felmy, A.; Goodman, D. W.; Grätzel, M.; Maciel, G.; McCarthy, M. I.; et al. *Chem. Rev.* **1999**, *99*, 77−174.
(18) Park, C.; Fenter, P.; Nagy, K.; Sturchio, N. *Phys. Rev. Lett.* **2006**, *97*, 016101.
(19) Peak, D. *J. Colloid Interface Sci.* **2006**, *303*, 337−345.
(20) Peak, D.; Sparks, D. L. *Environ. Sci. Technol.* **2002**, *36*, 1460−1466.
(21) Chen, C. C.; Coleman, M. L.; Katz, L. E. *Environ. Sci. Technol.* **2006**, *40*, 142−148.
(22) Criscenti, L. J.; Cygan, R. T.; Kooser, A. S.; Moffat, H. K. *Chem. Mater.* **2008**, *20*, 4682−4693.
(23) Fukushi, K.; Sverjensky, D. A. *Geochim. Cosmochim. Acta* **2007**, *71*, 1−24.
(24) Rietra, R. P. J. J.; Hiemstra, T.; van Riemsdijk, W. H. *Geochim. Cosmochim. Acta* **1999**, *63*, 3009−3015.
(25) Sverjensky, D. A.; Fukushi, K. *Environ. Sci. Technol.* **2006**, *40*, 263−271.
(26) Beattie, D. A.; Chapelet, J. K.; Grafe, M.; Skinner, W. M.; Smith, E. *Environ. Sci. Technol.* **2008**, *42*, 9191−9196.
(27) Rietra, R. P. J. J.; Hiemstra, T.; van Riemsdijk, W. H. *J. Colloid Interface Sci.* **2001**, *240*, 384−390.
(28) Muller, K.; Lefèvre, G. *Langmuir* **2011**, *27*, 6830−6835.
(29) Kester, D. R.; Duedall, I. W.; Connors, D. N.; Pytkowicz, R. M. *Limnol. Oceanogr.* **1967**, *12*, 176−179.
(30) Jubb, A. M.; Hua, W.; Allen, H. C. *Acc. Chem. Res.* **2012**, *45*, 110−119.
(31) Ishiyama, T.; Morita, A.; Miyamae, T. *Phys. Chem. Chem. Phys.* **2011**, *13*, 20965−20973.
(32) Miyamae, T.; Morita, A.; Ouchi, Y. *Phys. Chem. Chem. Phys.* **2008**, *10*, 1985−2124.
(33) Hopkins, A. J.; Schrodle, S.; Richmond, G. L. *Langmuir* **2010**, *26*, 10784−10790.
(34) Wise, M. E.; Baustian, K. J.; Tolbert, M. A. *Proc. Natl. Acad. Sci. U.S.A.* **2010**, *107*, 6693−6698.
(35) Yang, Z.; Bertram, A. K.; Chou, K. C. *J. Phys. Chem. Lett.* **2011**, *2*, 1232−1236.
(36) Miller, M. M. In *USGS Minerals Yearbook - Metals and Minerals*; United States Government Printing Office: Washington, DC, 2009; Vol. *1*.
(37) *CRC Handbook of Chemistry and Physics*; Haynes, W. M., Ed.; 92 - Internet Version 2012.; CRC Press: Boca Raton, FL, 2012.
(38) Schrodle, S.; Moore, F. G.; Richmond, G. L. *J. Phys. Chem. C* **2007**, *111*, 10088−10094.
(39) Becraft, K. A.; Richmond, G. L. *Langmuir* **2001**, *17*, 7721−7724.
(40) Jena, K. C.; Hore, D. K. *J. Phys. Chem. C* **2009**, *113*, 15364−15372.
(41) Kataoka, S.; Gurau, M. C.; Albertorio, F.; Holden, M. A.; Lim, S.-M.; Yang, R. D.; Cremer, P. S. *Langmuir* **2004**, *20*, 1662−1666.
(42) Ong, S.; Zhao, X.; Eisenthal, K. B. *Chem. Phys. Lett.* **1992**, *191*, 327−335.
(43) Jena, K. C.; Covert, P. A.; Hore, D. K. *J. Phys. Chem. Lett.* **2011**, *2*, 1056−1061.
(44) Du, Q.; Freysz, E.; Shen, Y. R. *Phys. Rev. Lett.* **1994**, *72*, 238−241.
(45) Yeganeh, M. S.; Dougal, S. M.; Pink, H. S. *Phys. Rev. Lett.* **1999**, *83*, 1179−1182.
(46) Ostroverkhov, V.; Waychunas, G. A.; Shen, Y. R. *Chem. Phys. Lett.* **2004**, *386*, 144−148.
(47) Zhang, L.; Tian, C.; Waychunas, G. A.; Shen., Y. R. *J. Am. Chem. Soc.* **2008**, *130*, 7686−7694.
(48) Malin, J. N.; Hayes, P. L.; Geiger, F. M. *J. Phys. Chem. C* **2009**, *113*, 2041−2052.
(49) Geiger, F. M. *Annu. Rev. Phys. Chem.* **2009**, *60*, 61−83.
(50) Mifflin, A. L.; Gerth, K. A.; Weiss, B. M.; Geiger, F. M. *J. Phys. Chem. A* **2003**, *107*, 6212−6217.
(51) Schrodle, S.; Moore, F. G.; Richmond, G. L. *J. Phys. Chem. C* **2007**, *111*, 8050−8059.
(52) Waldrup, S. B.; Williams, C. T. *J. Phys. Chem. B* **2006**, *110*, 16633−16639.
(53) Hatch, S. R.; Polizzotti, R. S.; Dougal, S.; Rabinowitz, P. *J. Vac. Sci. Technol. A* **1993**, *11*, 2232−2238.
(54) Schrödle, S.; Richmond, G. L. *J. Phys. D: Appl. Phys.* **2008**, *41*, 033001.
(55) Lambert, A. G.; Davies, P. B.; Neivandt, D. J. *Appl. Spectrosc. Rev.* **2005**, *40*, 103−145.
(56) Jubb, A. M.; Hua, W.; Allen, H. C. *Annu. Rev. Phys. Chem.* **2012**, *63*, 6.1−6.24.
(57) Lobau, J.; Wolfrum, K. *J. Opt. Soc. Am. B* **1997**, *14*, 2505−2512.
(58) Wiesner, A. D.; Katz, L. E.; Chen, C. C. *J. Colloid Interface Sci.* **2006**, *301*, 329−332.
(59) Johnson, C. M.; Tyrode, E. *Phys. Chem. Chem. Phys.* **2005**, *7*, 2635−2640.
(60) Pye, C. C.; Rudolph, W. W. *J. Phys. Chem. A* **2001**, *105*, 905−912.
(61) Rudolph, W. W.; Irmer, G.; Hefter, G. T. *Phys. Chem. Chem. Phys.* **2003**, *5*, 5253−5261.
(62) Adamson, A. W.; Gast, A. P. *Physical Chemistry of Surfaces*, 6th ed.; Wiley-Interscience: New York, NY, 1997.
(63) Berenblut, B. J.; Dawson, P.; Wilkinson, G. R. *Spectrochim. Acta, Part A* **1973**, *29A*, 29−36.